

Bandwidth-controlled Mott transition in κ -(BEDT-TTF) $_2$ Cu[N(CN) $_2$]Br $_x$ Cl $_{1-x}$: Optical studies of correlated carriers

Michael Dumm, Daniel Faltermeier, Natalia Drichko, and Martin Dressel

1. Physikalisches Institut, Universität Stuttgart, Pfaffenwaldring 57, D-70550 Stuttgart Germany

Cécile Mézière and Patrick Batail

*Laboratoire CIMMA, UMR 6200 CNRS-Université d'Angers, Bât. K,
UFR Sciences, 2 Boulevard Lavoisier, F-49045 Angers, France*

(Dated: October 28, 2018)

In the two-dimensional organic charge-transfer salts κ -(BEDT-TTF) $_2$ Cu[N(CN) $_2$]Br $_x$ Cl $_{1-x}$ a systematic variation of the Br content from $x = 0$ to 0.9 allows us to tune the Mott transition by increasing the bandwidth. At temperatures below 50 K, an energy gap develops in the Cl-rich samples and grows to approximately 1000 cm $^{-1}$ for $T \rightarrow 0$. With increasing Br concentration spectral weight shifts into the gap region and eventually fills it up completely. As the samples with $x = 0.73, 0.85$ and 0.9 become metallic at low temperatures, a Drude-like response develops due to the coherent quasiparticles. Here, the quasiparticle scattering rate shows a ω^2 dependence and the effective mass of the carriers is enhanced in agreement with the predictions for a Fermi liquid. These typical signatures of strong electron-electron interactions are more pronounced for compositions close to the critical value $x_c \approx 0.7$ where the metal-to-insulator transition occurs.

PACS numbers: 71.30.+h, 71.10.Hf, 74.70.Kn, 74.25.Gz

I. INTRODUCTION

One of the most intriguing issues in condensed-matter physics is the transition from a metal to an insulator driven by electronic correlations. Why does an electron in a crystal change from itinerant to localized behavior when a control parameter such as magnetic field, doping or pressure is varied? For a system with a half-filled conduction band this problem is known as the Mott transition, one of the central problems of strongly-correlated electrons.¹ While studies of the influence of electron-electron interactions in materials with open d and f electron shells have a long history,^{2,3,4} only recently it was realized that also in molecular conductors (where the charges originate from molecular orbitals) electronic correlations are very significant.^{5,6,7,8,9,10} In transition-metal oxides, the Coulomb interaction is crucial for any understanding of the unconventional metallic and superconducting properties as well as the vicinity to magnetic order; this is most pronounced in the underdoped cuprates.⁴ However, in many regards organic conductors turn out to be superior model systems to study certain effects of electron-electron interaction since their properties can be more easily tuned by (physical or chemical) pressure. Varying U/t , where U is on-site repulsion and t is a transfer integral, opens the road to the bandwidth-controlled Mott transition.

The family of half-filled organic conductors κ -(BEDT-TTF) $_2X$ (anions $X = \text{Cu}(\text{CN})_3, \text{Cu}[\text{N}(\text{CN})_2]\text{Cl}, \text{Cu}[\text{N}(\text{CN})_2]\text{Br}, \text{Cu}(\text{SCN})_2$, and I_3)¹¹ has a particularly rich phase diagram as a function of pressure and temperature as depicted in Fig. 1. The abscissa of this phase diagram can be interpreted as the variation of the relative Coulomb interaction U/t . Similar to external pressure, a variation of anions also changes the bandwidth

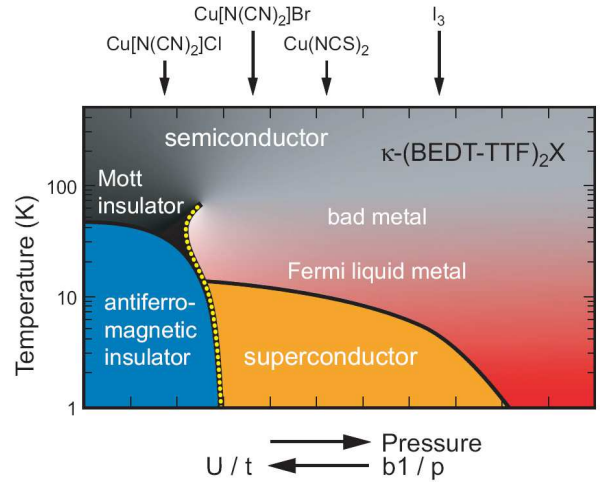


FIG. 1: Schematic phase diagram of κ -(BEDT-TTF) $_2X$. The on-site Coulomb repulsion with respect to the hopping integral U/t can be tuned either by external pressure or modifying the anions X . The arrows indicate the approximate position of κ -phase salts with $X = \text{Cu}[\text{N}(\text{CN})_2]\text{Cl}$, $\text{Cu}[\text{N}(\text{CN})_2]\text{Br}$, $\text{Cu}(\text{NCS})_2$, and I_3 at ambient pressure, respectively. The bandwidth controlled phase transition between the insulator and the Fermi liquid/superconductor can be explored by gradually replacing Cl by Br in κ -(BEDT-TTF) $_2\text{Cu}[\text{N}(\text{CN})_2]\text{Br}_x\text{Cl}_{1-x}$. Here c and a are the lattice parameters; b_1 and p indicate intra- and interdimer transfer integrals, respectively.

and thus reduces U/t . For large values of U/t the half-filled system becomes a Mott insulator. This behavior is observed in κ -(BEDT-TTF) $_2\text{Cu}[\text{N}(\text{CN})_2]\text{Cl}$: at ambient conditions the narrow-gap semiconductor gradually gets insulating when cooled below 50 K. The application of external pressure shifts the compound across the phase

boundary. It becomes metallic and even undergoes a superconducting transition, very similar to the Br analog at ambient pressure. Recently, the critical behavior in the vicinity of the metal-insulator transition and the critical endpoint was thoroughly investigated by dc measurements under external pressure and magnetic field.^{12,13,14} In the present study we gradually substitute Cl by the isovalent Br in the anion layers and obtain the series κ -(BEDT-TTF)₂Cu[N(CN)₂]Br_xCl_{1-x} crossing over from the Mott insulator with antiferromagnetic ground state (Cl-compound) to a Fermi liquid which becomes superconducting at $T_c = 12$ K (Br-compound).

Over the last decade dynamical mean-field theory has been established as a powerful tool to study the physical properties of highly-correlated electron systems.^{15,16} To understand the properties of κ -phase BEDT-TTF-based salts, Kino and Fukuyama¹⁷ suggested to model them by a triangular lattice of BEDT-TTF dimers with one hole per site and hopping between the dimer sites t_1 and t_2 and on-site repulsion U . A Mott-type metal-insulator transition occurs at some critical value of the relative Coulomb repulsion $(U/t)_c$. Merino and McKenzie^{18,19} evaluated the transport properties of the metallic side of the phase diagram of these half-filled systems using a dynamical mean-field treatment (DMFT) of the Hubbard model with strong on-site Coulomb repulsion $U \approx W$ (with $W = 10t$ being the bandwidth for the frustrated square lattice in tight-binding approximation). They show that the optical conductivity exhibits a zero-frequency mode (Drude peak) at low temperatures, while it is suppressed above some coherence temperature T_{coh} , meaning close to a Mott metal-insulator transition the quasiparticles are destroyed for $T > T_{\text{coh}}$.

Optical investigations give a respective experimental insight into the dynamics of the conduction electrons, including the existence of the coherent and incoherent quasiparticle response.^{20,21,22,23,24,25,26} In Ref. 27 we presented the reflectivity data (frequency range: 50 to 10 000 cm⁻¹, temperature range: 5 to 300 K) received on single crystals of κ -(BEDT-TTF)₂Cu[N(CN)₂]Br_xCl_{1-x} ($x = 0, 0.4, 0.73, 0.85, \text{ and } 0.9$). The interpretation of the frequency-dependent conductivity $\sigma_1(\omega)$ which is shown in the left panels of Fig. 2 for $E \parallel c$ was performed in terms of two contributions: charge transfer inside the dimer “lattice sites” and interdimer charge transfer by correlated charge carriers. At ambient temperature the frequency-dependent conductivity $\sigma_1(\omega)$ is dominated by a broad absorption peak located at frequencies around 2000 - 3500 cm⁻¹. Down to $T = 50$ K no Drude-like contribution to the optical conductivity is present although the crystals are moderately good conductors. At even lower temperatures a zero-frequency contribution is observed for κ -(BEDT-TTF)₂Cu[N(CN)₂]Br_xCl_{1-x} with $x = 0.73, 0.85, \text{ and } 0.9$, but not for the lower concentrations of Br where an energy gap opens at the metal-insulator transition. Using the cluster model suggested by Rice, Yartsev and coworkers,^{28,29,30} we showed that the electronic band with a maximum at around 3500 cm⁻¹

($E \parallel c$) and the narrow features at frequencies of BEDT-TTF molecular vibrations are due to the charge transfer within a dimer coupled to A_g vibrations of BEDT-TTF. This analysis permits to disentangle the intradimer and interdimer carriers contributions to the spectra, as demonstrated Refs. 27 and 31 whereas the latter account for the Mott-Hubbard physics due to strong electronic correlations.

In the present study we closer inspect the transition into the Mott-insulating state in κ -(BEDT-TTF)₂Cu[N(CN)₂]Br_xCl_{1-x} driven either upon lowering the temperature or decrease of chemical pressure. We confine ourselves to a detailed analysis of one of the in-plane polarizations (the c -axis) where it is easier to disentangle the different contributions to the spectra. However, an analysis of the a -axis spectra leads to qualitatively comparable results; the response of the strongly-correlated carriers is basically isotropic in the conducting plane.²⁷ Starting with the proposed density of states, we will discuss the following aspects of the Mott-Hubbard model system: the appearance of an energy gap and a quasi-particle peak at low temperatures and their evolution as function of temperature and effective Coulomb interaction, the suppression of the spectral weight across the transition, and the Fermi-liquid response of the metallic state in the vicinity of the Mott transition.

II. RESULTS AND DISCUSSION

A. Analysis of the complete spectra

1. Redistribution of spectral weight

Figs. 2(a)-(e) show the optical conductivity for $E \parallel c$ in the measured frequency range. Within this range we observe all the studied processes, the intradimer transitions and the interdimer transitions which show up as Hubbard bands and Drude-like peak, depending on the compound and temperature. The relatively distinct drop in reflectivity around 4000 to 5000 cm⁻¹ shown in Ref. 27 infers that the optical conductivity up to these frequencies is governed by the electrons in the conduction band formed by the overlap of BEDT-TTF orbitals in the layer. The one-dimensional tight-binding model illustrates the proportionality between the value of the spectral weight and transfer integral t : $\int_0^\infty \sigma_1(\omega) d\omega = \frac{2td^2e^2}{\hbar^2V_m} \sin\{\frac{\pi}{2}\rho\}$, where d is the inter-molecular distance, V_m denotes the volume per molecule, and the electrons per site are given by ρ . Due to the triangular lattice, there is no single transfer integral that can define the width of the band; nevertheless the equation still gives the correct idea, that up to about 6000 cm⁻¹ we are dealing with intra-band transitions.³²

The frequency-dependent spectral weight is given by

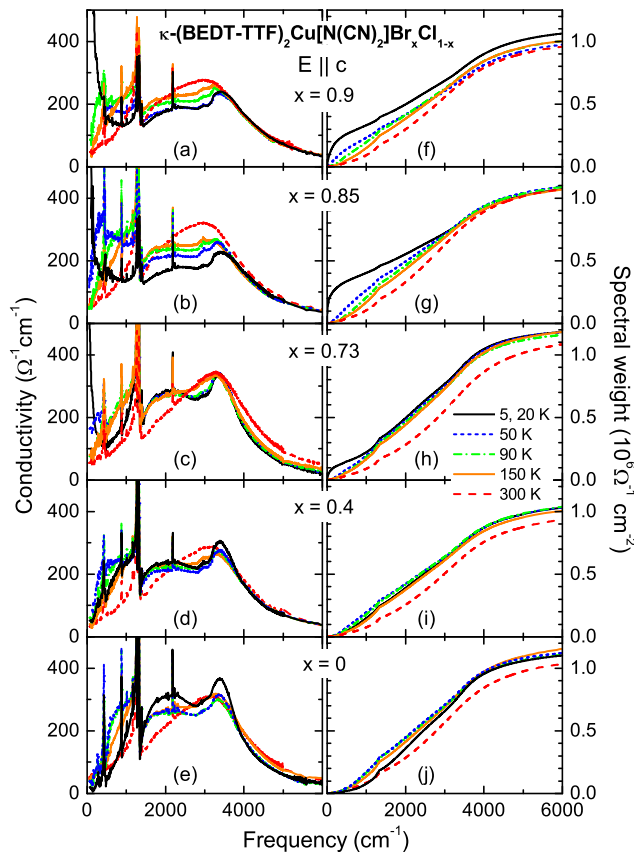


FIG. 2: (Color online) Left frames: experimental spectra of the real part of the complex conductivity σ_1 of κ -(BEDT-TTF) $_2$ Cu[N(CN) $_2$]Br $_x$ Cl $_{1-x}$ for the in-plane $E \parallel c$ measured at different temperatures; right frames: spectral weight as a function of cut-off frequency $\omega_c/(2\pi c)$ calculated according to Eq. (1). From the top to the bottom panels, (a) - (e) and (f) - (j) respectively, the Br content is reduced from 0.9 to 0.

the integral³³

$$I_\sigma(\omega_c) = \int_0^{\omega_c} \sigma_1(\omega) d\omega = \frac{\pi e^2}{2m_{\text{sum}}^*} n(\omega_c) \quad , \quad (1)$$

where ω_c is a cut-off frequency and m_{sum}^* an effective mass which is equal to the optical band mass $m_{b,\text{opt}}$ in the non-interacting case; $n(\omega_c)$ indicates the density of carriers contributing to the conductivity up to ω_c . First of all, within the experimental uncertainty the spectral weight is approximately the same for all temperatures and Br concentrations when going up to $\omega_c/(2\pi c) = 6000 \text{ cm}^{-1}$ or higher,³⁴ as demonstrated in Fig. 2(f)-(j). The conservation of the spectral weight within the band suggests that we can ignore the higher-frequency interband transitions and focus our attention on the spectral range below 6000 cm^{-1} . Within this region, the frequency redistribution of the spectral weight with varying temperature and Br concentration shows from which energy range what kind of charge carriers contribute to the optical response [Eq. (1)]. In conventional metals most of the optical weight is concentrated in the Drude peak and $I_\sigma(\omega_c)$

should quickly saturate with frequency, which is not the case in the studied compounds.

The steps around 500 and 1200 cm^{-1} in all the $I_\sigma(\omega_c)$ curves are due to the strong emv-coupled molecular vibrations. Most important, the distribution of the spectral weight significantly changes for the different samples. With lowering the temperature, a shift to lower frequencies occurs that is much more pronounced in the crystals with high Br content. In the salts with $x = 0.85$ and 0.9 , a strong increase of the spectral weight is observed below $\omega_c/(2\pi c) = 1000 \text{ cm}^{-1}$ and $T = 150 \text{ K}$, while in κ -(BEDT-TTF) $_2$ Cu[N(CN) $_2$]Br $_{0.73}$ Cl $_{0.27}$ this shift is less prominent. Contrary to this tendency, below 150 K the far- and mid-infrared spectral weight decreases in the samples with $x = 0.4$ and 0 . It should be pointed out that the difference between the temperature behavior of the samples is observed only below 3000 cm^{-1} , i.e. in the spectral region of the correlated-carriers contribution, which will be analyzed below.

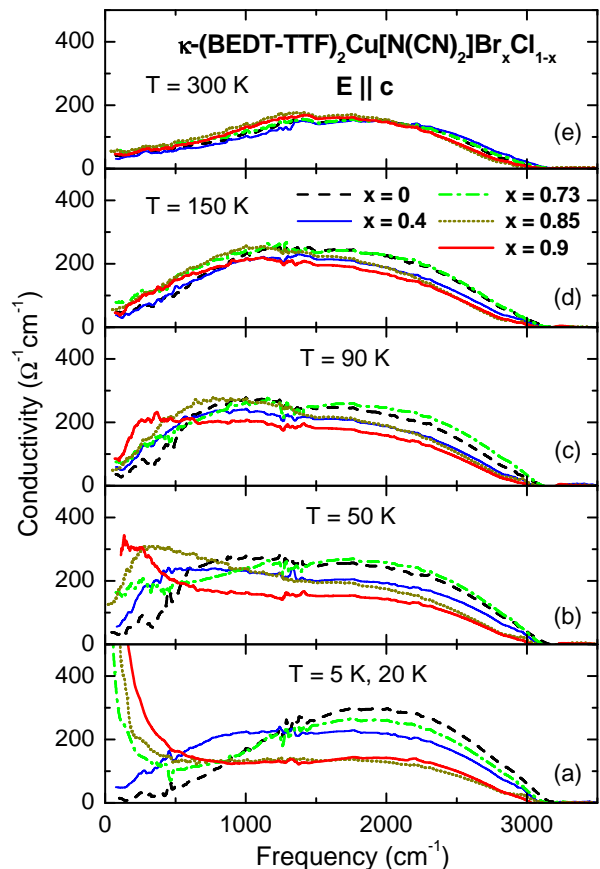


FIG. 3: (Color online) Frequency dependence of the conductivity σ_1 ($E \parallel c$) due to correlated charge carriers after the contributions from intradimer transitions and vibrational modes are subtracted. The frames (a) - (e) show spectra of κ -(BEDT-TTF) $_2$ Cu[N(CN) $_2$]Br $_x$ Cl $_{1-x}$ with different Br concentrations x at various temperatures as indicated.

2. Mott-Hubbard system

For the inspection of the dynamics of the correlated charge carriers, the features due to the intradimer transitions were extracted from the experimental spectra of both σ_1 and σ_2 in a Kramers-Kronig consistent way, following the ideas and procedure developed and discussed in Refs.27 and 31; the resulting σ_1 spectra are presented in Fig. 3. At lowest temperatures shown in panel (a) of Fig. 3, we can distinguish two main contributions: (i) a finite-frequency part (centered around 2000 cm^{-1}), which is the sole contribution in the case of low Br content $x = 0$ and 0.4 , and which becomes weaker as x increases; (ii) a zero-frequency peak for the large- x samples due to coherent particle response. These two basic features are in good agreement with a theoretical prediction for a Mott-Hubbard system³⁵ as sketched in Fig. 4(b): a Drude-like peak at $\omega = 0$, and a broad absorption band at about U ; while we do not observe a mid-infrared band at $U/2$ in our spectra. Assuming a frustrated square lattice as depicted in Fig. 4(a) with hopping parameters $t_1 = 0.024\text{ eV}$ and $t_2 = 0.03\text{ eV}$, and $U = 10|t_2| = 0.3\text{ eV}$, Merino and McKenzie^{18,19} could quantitatively describe the experimental findings. The broad band at 2000 cm^{-1} is attributed to electronic transitions between the two Hubbard bands. Interestingly, the position of the Hubbard transition does not change with temperature and upon Br substitution. This implies that it does not depend on the transfer integral t_2 and the degree of frustration t_1/t_2 , but only on the Coulomb interaction U that is identical for all materials.

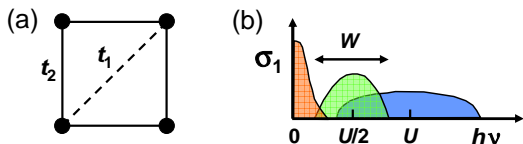


FIG. 4: (a) Anisotropic triangular lattice used in theoretical calculations of the electronic properties; the ratio $t_1/t_2 = 0.8$. (b) A schematic view of conductivity spectrum predicted by DMFT for a metallic compound close to the Mott transition.

If the temperature increases [panels (b) to (c) of Fig. 3], the coherent carriers peak disappears for the high Br concentrations, showing that no coherent transport is possible anymore. This results in the so-called “bad-metal” behavior, where the dc resistivity still increases with temperature up to the maximum at about 100 K but no band-like transport occurs. An evaluation of the Hubbard model by dynamical mean-field theory reproduces the signatures of the gradual destruction of quasiparticles as the temperature passes T_{coh} . At 150 K and above [panels (d) and (e) of Fig. 3], independently of the Br content a semiconducting behavior is recovered which is characterized by a negative slope of ρ versus T (Fig. 3 of Ref. 27).

While these main features of the metallic samples are in good agreement with theory, the overall picture of the

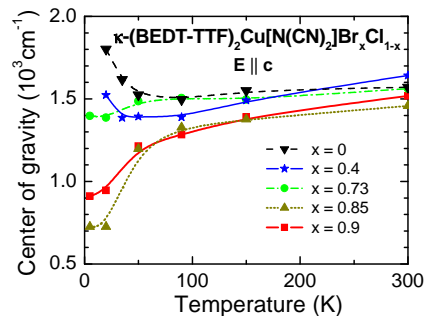


FIG. 5: (Color online) Shift of the center of gravity in the conductivity spectra of the correlated charge carriers with temperature for different x in κ -(BEDT-TTF)₂Cu[N(CN)₂Br_xCl_{1-x}] for $E \parallel c$. The lines correspond to spline fits.

conductivity spectra of the correlated carriers as function of temperature and Br content x adds new information. At high temperatures, $\sigma_1(\omega)$ does not depend much on Br content x , and a shift of spectral weight to lower frequencies is observed for *all* the compounds when going from 300 K to 150 K . The behavior becomes qualitatively different at 50 K as the higher-frequency contribution gets noticeably reduced and a peak emerges below 500 cm^{-1} for $x = 0.9, 0.85,$ and 0.73 . At lowest temperature, 20 K and 5 K , this peak evolves into the coherent carriers peak; the finite-frequency band becomes so reduced that it can be barely distinguished from the higher-frequency wing of the Drude contribution. For lower Br concentration, the intensity of the transitions between the Hubbard bands at about 2000 cm^{-1} remains the same, though the contribution at about 300 cm^{-1} rises as temperature increases above 35 K and the systems cross over into the semiconducting state.

The spectral-weight shift towards lower frequencies on cooling from 300 to 50 K can be interpreted as a signature of “getting closer” to a metallic state; this is illustrated by the monotonic decrease of the center of gravity of the spectra shown in Fig. 5 as a function of temperature, where the values are calculated from Fig. 3. At lower temperatures the behavior is distinctively different: the shift becomes more pronounced for the metallic samples with $x = 0.85$ and 0.9 , while the opening of the Mott-Hubbard gap causes an upward shift of the center of gravity for $x = 0$ and 0.4 . Interestingly, the sample with $x = 0.73$ is positioned between both limiting cases, but at the lowest temperatures the coherent particle response appears.

B. Density of states

For further understanding and comparison to the theory, we sketch in Fig. 6 the density of states (DOS) as proposed from the above discussion of our data. We chose three typical temperature (low temperature, around 50 K , and high temperature) and correlation regions (high

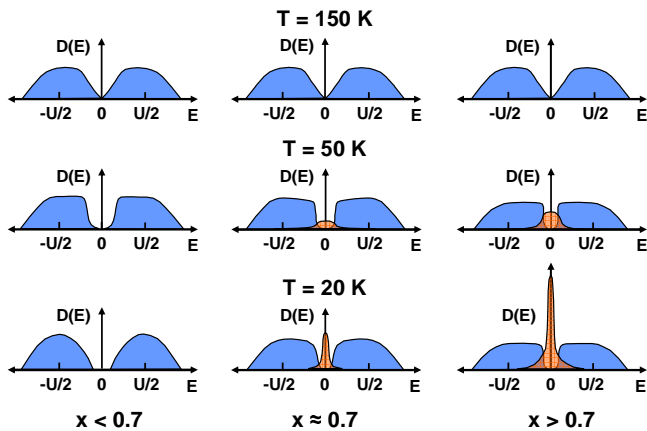


FIG. 6: (Color online) Density of states at $T = 150$ K, 50 K, and 20 K as proposed for the low Br-doped compounds ($x < 0.7$), the crystal with $x \approx 0.7$, and the highly Br-doped samples ($x < 0.7$) from the optical conductivity. The zero-frequency mode is shown in orange color and the finite-frequency modes in blue color. The temperatures represent the metallic or Mott-insulating region (20K), the narrow-gap semiconducting high-temperature region (150K) and the crossover regime between the former which is often referred to as “bad-metal” or “bad-semiconductor” region.

Br content, $x = 0.73$, and low Br content) in order to cover all relevant parts of the phase diagram (Fig. 1). The upper and lower Hubbard bands and, accordingly, the optical transitions between them are present for all the temperatures and correlation values. At 150 K and higher temperatures these bands are more or less symmetric and seem to extend down to zero frequency. When temperature is decreased down to 90 and 50 K, respectively, the center of gravity of the finite-frequency bands moves gradually to lower frequencies (Fig. 5). From the optical conductivity (Fig. 3) it is obvious that the spectral weight shifts from the mid-infrared into the far-infrared region, however, the appearance of the strong absorption edge below 500 cm^{-1} signals a much more abrupt onset of the absorption band at these temperatures. The onset frequency is smaller for the compounds with lower correlation values (higher Br dopings) where the sharp edge of the finite-frequency absorptions and the emerging quasiparticle peak add up to a maximum in the total DOS just above the gap; such kind of behavior is predicted by cluster DMFT calculations.^{36,37,38} At lowest temperatures, the coherent carriers peak dominates the DOS close to the Fermi energy in the salts with $x > 0.7$ which corresponds to the Drude-like response in the optical conductivity.

The calculations in Refs. 36,37,38 were performed for low temperatures in the Mott-insulating phase close to the Mott transition in a half-filled two-dimensional system. They suggested that besides the Hubbard bands situated at $|E| = U/2$, there might be more contributions to the broad bands at $|E| > 0$. A particular attention was given to short-range correlations which cause an

additional band in the spectra. In contrast to single-site calculations, cluster DMFT reveals these short-range correlations which reduce the critical Coulomb repulsion U ; most important in this context, additional low-frequency excitations are expected due to local singlet formation.

There remains a considerable discrepancy between our experimental data and single-site DMFT calculations: the absence of the $U/2$ peak related to excitations from the Hubbard band to the quasiparticle peak [compare Figs.3(a) and 4(b)]. Although there is an overlap between the higher-frequency part of the Drude peak and the broad band of transitions between Hubbard bands in the experimental data which might hide a weak absorption feature, it is obvious that this contribution is not as strong as predicted by theory. However, in this regard it is important to mention that optical experiments do not resolve the k -dependence which causes a smearing of the spectral features. Additionally, the single-band approach by the theory might be a reason for the deviations.

C. Metal-insulator transition

1. Energy gap

A characteristic signature of the metal-insulator transition is the opening of an energy gap in the excitation spectrum. Our experiments on crystals with different Br-concentrations provided the opportunity to probe the transition into the Mott-insulating state as function of temperature and correlation: at low Br content, a transition from a narrow-gap semiconducting³⁹ into a Mott-insulating state occurs on lowering the temperature, while at a fixed low temperature the system crosses over from a metallic into a Mott-insulating state on the increase of the relative Coulomb repulsion U/t .

As demonstrated in Fig. 7(a), the pristine κ -(BEDT-TTF)₂Cu[N(CN)₂]Cl crystal shows typical signatures of a Mott insulator with an energy gap gradually growing as the temperature drops below 50 K. There is no clear-cut definition of the gap value: the extrapolation to zero conductivity seems to be arbitrary. The fit of the conductivity spectrum by a Lorentz oscillator leads to frequencies which are much too high. An alternative way is to consider the energy range where the spectral weight is low. If we choose the frequency Δ for which the spectral weight reaches $\int_0^\Delta \sigma_1(\omega) d\omega = 50000 \text{ } \Omega^{-1} \text{ cm}^{-2}$, i.e. about 10% of the total spectral weight, we obtain a 50 K-gap value of $\Delta/2\pi c = 570 \text{ cm}^{-1}$. As already pointed out by Kornelsen *et al.*,²¹ the gap grows almost linearly with decreasing temperature (by about $10 \text{ cm}^{-1}/\text{K}$) indicating a second-order transition. At 20 K, we obtain $\Delta/2\pi c = 900 \text{ cm}^{-1}$ and for $T \rightarrow 0$ we extrapolate to about 1000 cm^{-1} ; this is in good agreement with the previous estimates. The result suggests that for increasing temperature the carriers in κ -(BEDT-TTF)₂Cu[N(CN)₂]Cl are less localized. The gap diminishes continuously with rising temperature as expected for a mean-

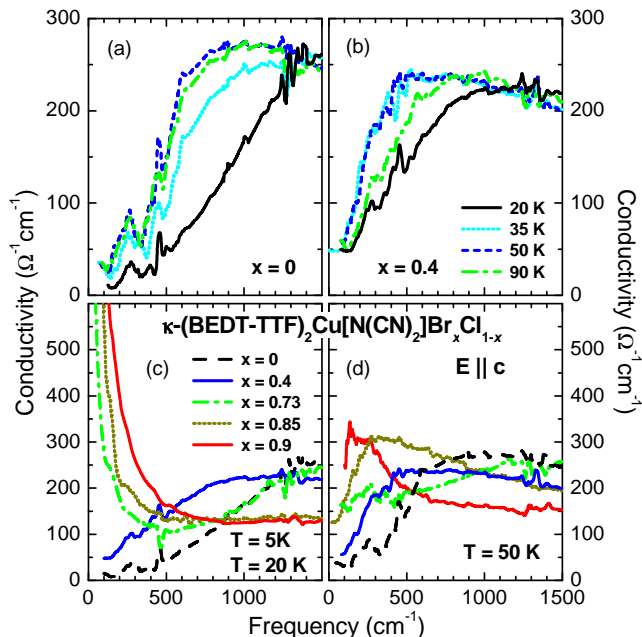


FIG. 7: (Color online) Comparison of the development of the optical gap with changing the Br concentration and temperature for $E \parallel c$. The panels show the frequency-dependent conductivity σ_1 after subtracting contributions due to localized charge carriers and vibrational modes. (a) and (b): $\sigma_1(\omega)$ $T = 90$ K, 50 K, 35 K, and 20 K of for $x = 0$ (a) and $x = 0.4$ (b). (c) and (d): dependence of $\sigma_1(\omega)$ on Br concentration for lowest $T = 20$ K ($x = 0$ and 0.4) and $T = 5$ K ($x = 0.73, 0.85,$ and 0.9) (c) and $T = 50$ K (d).

field transition, but does not disappear completely since the material is a narrow-gap semiconductor at high temperatures.

For the sample with $x = 0.4$ (Fig. 7(b)) the conductivity in the low-frequency region is still suppressed below 50 K, however, the gap value is significantly smaller than in the pure Cl compound. Using the same method as above, we obtain $\Delta/(2\pi c) = 400$ cm^{-1} at 50 K and $\Delta/(2\pi c) = 580$ cm^{-1} at 20 K, or for $T \rightarrow 0$ we extrapolate to about 650 cm^{-1} . In agreement with the present observation, a considerable reduction of the energy gap was recently predicted by cluster DMFT when U/t is reduced.^{36,37,38} Most of the reduction is attributed to the presence of two strong peaks in the spectral functions at the gap edge induced by short-range antiferromagnetic correlations in addition to the Hubbard bands. However, the broad region of enhancement in the optical conductivity of $\kappa\text{-(BEDT-TTF)}_2\text{Cu}[\text{N}(\text{CN})_2]\text{Br}_{0.4}\text{Cl}_{0.6}$ compared to the pristine Cl compound below 1250 cm^{-1} (Fig. 3(a)) indicates that these bands are not as sharp as anticipated by the theoretical calculations.

The complete picture at the lowest temperature is demonstrated in Fig. 7(c) where the conductivity of $\kappa\text{-(BEDT-TTF)}_2\text{Cu}[\text{N}(\text{CN})_2]\text{Br}_x\text{Cl}_{1-x}$ is plotted for $x = 0, 0.4, 0.73, 0.85,$ and 0.9. When the Br concentration increases above $x = 0.4$, the optical gap is not substantially

reduced further but gradually filled in; a strong Drude contribution develops. Indeed, with larger Br substitution, the relative Coulomb repulsion U/t is reduced. As it gets below a critical point (between $x = 0.4$ and 0.73), a first-order transition occurs, where the density of states at the Fermi level is supposed to rise abruptly to a finite value.⁴⁰ The coherent quasiparticles form a Drude-like zero-frequency peak; this contribution will be further analyzed in the following Sec. II C 2.

The panel (d) of Fig. 7 focusses on the optical conductivity of $\kappa\text{-(BEDT-TTF)}_2\text{Cu}[\text{N}(\text{CN})_2]\text{Br}_x\text{Cl}_{1-x}$ at $T = 50$ K, which is slightly above the Mott-insulating or coherence temperature, respectively. Accordingly, both the Mott gap in the low Br-doped compounds and the Drude contribution in the salts with high Br content, are suppressed. However, the conductivity below 500 cm^{-1} is still much higher for the metallic compounds with $x = 0.85$ and 0.9, showing a wide peak at about 300 cm^{-1} as discussed in the previous section.

2. Coherent quasiparticle response

According to the Drude model, the optical response of the free carriers in a conventional metal is restricted to a zero-frequency mode. Its spectral weight $\int \sigma_1(\omega) d\omega$ is temperature independent. As the temperature is lowered and phonon scattering freezes out, the Drude peak becomes narrower and $\sigma(T)$ increases accordingly. Contrary, in heavy fermions which are benchmark systems for the physics of strongly-correlated electrons the spectral weight of the zero-frequency contribution typically condenses when T drops below some coherence temperature, because the effective mass $m^*(T)$ increases due to electron-electron interactions.⁴¹ At a metal-insulator transition (caused by electronic correlations or other reasons) the Drude spectral weight abruptly vanishes $D(T) \rightarrow 0$.

In order to get information on the correlation and temperature evolution of the coherent quasiparticle response in $\kappa\text{-(BEDT-TTF)}_2\text{Cu}[\text{N}(\text{CN})_2]\text{Br}_x\text{Cl}_{1-x}$ we calculate the spectral weight of the low-frequency part of the spectra shown in Fig. 3. Since the spectra exhibit a minimum in the range between 500 and 800 cm^{-1} for any $x \geq 0.73$ at low temperatures [Fig. 3(a)], we have picked $\omega_c/(2\pi c) = 700$ cm^{-1} as a possible cut-off frequency. The temperature dependence of $I_{\sigma, \omega_c=700 \text{ cm}^{-1}}$ is plotted in Fig. 8. For all values of x , the intensity of the low-frequency spectral weight increases as the temperature is lowered from room temperature down to 50 K. Reducing T even further, $I_{\sigma, \omega_c=700 \text{ cm}^{-1}}$ drops significantly for the $x = 0$ and 0.4 samples because the Mott-Hubbard gap opens as the insulating state is entered. As the Drude peak develops at $T \leq 50$ K, the metallic samples ($x \geq 0.73$) exhibit a steady enhancement $I_{\sigma, \omega_c=700 \text{ cm}^{-1}}$, the effect is strongest in the samples containing the highest amount of Br.

In an alternative approach, the zero-frequency mode

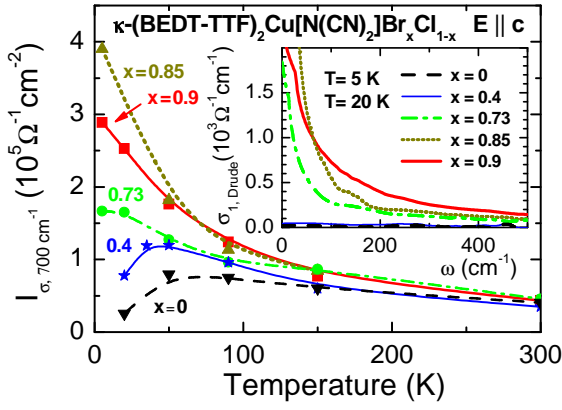


FIG. 8: (Color online) Temperature dependence of the spectral weight I_σ of the conduction electrons in κ -(BEDT-TTF)₂-Cu[N(CN)₂]Br_xCl_{1-x} with $x = 0, 0.4, 0.73, 0.85,$ and 0.9 calculated via integration of σ_1 plotted in Fig. 3 up to $\omega_c/(2\pi c) = 700 \text{ cm}^{-1}$ for $E \parallel c$. The lines are guides to the eye. The inset shows the Drude conductivity $\sigma_{1,\text{Drude}}$ obtained after subtraction of all finite-frequency modes at lowest temperatures ($T = 20 \text{ K}$ for $x = 0$ and 0.4 and $T = 5 \text{ K}$ for $x = 0.73, 0.85,$ and 0.9).

can be disentangled from the transitions between the Hubbard bands by subtracting the latter. It is obvious from Fig. 3 that this is only possible at lowest temperatures where both contributions are well separated. The far-infrared spectral range of the resulting Drude conductivity $\sigma_{1,\text{Drude}}$ is shown in the inset of Fig. 8. Interestingly, the width of the Drude peak is much smaller for $x = 0.85\%$ compared to $x = 0.9\%$ while the amplitude, i.e., the dc conductivity, is much higher in the former.⁴²

The strength of the coherent quasiparticle response can be estimated from the relative Drude weight D/D_0 (Fig. 9) where D is the spectral weight I_σ of the quasiparticle peak obtained by integration of the data shown in the inset of Fig. 8 and D_0 the total spectral weight of the coherent carriers shown in Fig. 10. From the simplest linear interpolation, two regimes can be identified at lowest temperature as illustrated in Fig. 9. A Drude response is found only for $x > 0.7$, it rapidly grows in weight as the Br content increases, i.e., the relative strength of the Coulomb interaction U/t decreases. The ratio D/D_0 , should exhibit a jump at $(U/t)_c$.^{43,44} The limited number of Br concentrations x available for our study does not allow us to give a definite number for D/D_0 at the critical point. Since the phase transition at the critical $(U/t)_c$ is of first order, Bulla *et al.*⁴⁰ predicted that the abrupt change of the Drude weight $D(x)$ even shows some hysteresis which might be checked in the future by very precise far-infrared spectroscopy with continuous variation of the external pressure. Actually, in transport measurements as function of pressure a hysteresis between increasing and decreasing pressure sweeps was reported.^{13,14}

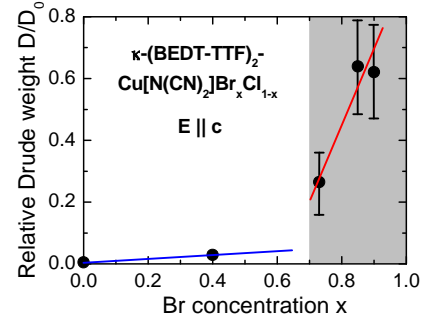


FIG. 9: (Color online) Ratio of the low-temperature Drude spectral weight $D(x)$ to the total spectral weight of the correlated charge carriers $D_0(x)$ at 20 K ($x = 0$ and 0.4) and $T = 5 \text{ K}$ ($x = 0.73, 0.85, 0.9$). The solid lines are guides to the eyes and help to identify the Mott-insulating and metallic regimes (grey area) with a boundary around $x_c = 0.7$.

3. Suppression of the spectral weight across the transition

The optical-spectral-weight redistribution can be analyzed more precisely based on the restricted f-sum rule for the effective one-band Hubbard model:⁴⁵

$$\int_0^\infty \sigma_1(\omega) d\omega = \frac{\pi N}{2D} \frac{e^2 d^2}{\hbar^2 c_0 M \Omega} \langle -E_{\text{kin}} \rangle, \quad (2)$$

where D is the dimension and N is the total number of carriers per dimer. M is the number of dimers in the crystal, Ω the volume per (BEDT-TTF)₂ dimer and d the lattice parameter. Eq. (2) brings a dynamical quantity, which probes the optical transitions in the system, together with a ground-state quantity, the total kinetic energy of the many-body system (the Hubbard model) and depends on temperature T and Coulomb repulsion U in contrast to the full sum rule given in Eq. (1).

As we already have shown in Ref. 19, the spectral weight of the system is indeed suppressed: while for a non-interacting system the DMFT calculation gives a result for the spectral weight of $\frac{N}{4D} \frac{e^2 d^2}{\hbar^2 c_0 M \Omega} \langle -E_{\text{kin}} \rangle_0 = 9.16 \cdot 10^5 \text{ } \Omega^{-1} \text{ cm}^{-2}$, the calculated spectral weight of a system with $U = 0.3 \text{ eV}$ is $5.8 \cdot 10^5 \text{ } \Omega^{-1} \text{ cm}^{-2}$ in good agreement with the experimental result $6.4 \cdot 10^5 \text{ } \Omega^{-1} \text{ cm}^{-2}$ obtained for κ -(BEDT-TTF)₂Cu[N(CN)₂]Br_{0.73}Cl_{0.27} with a cut-off frequency in the order of U . A similar effect of suppressed E_{kin} is observed in optical experiments on cuprate superconductors^{46,47} which are considered to be doped Mott insulators.

In Fig. 10 we present for the first time the development of the spectral weight of the correlated charge carriers across the metal-insulator transition at low temperatures. For all compounds, at frequencies of the order of U [i.e., $\omega/(2\pi c) \gtrsim 3000 \text{ cm}^{-1}$] the spectral weight saturates. Due to the strong electronic correlations it is considerably reduced,¹⁹ this effect gets stronger with increasing correlations and for the insulating compounds $x < 0.73$ a further suppression is observed. Here, the contribution of the zero-frequency mode to the spectral

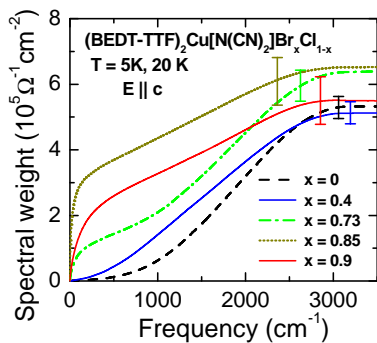


FIG. 10: (Color online) Spectral-weight distribution for κ -(BEDT-TTF) $_2$ Cu[N(CN) $_2$]Br $_x$ Cl $_{1-x}$ at low temperature. The spectral weight is redistributed as one approaches the transition to the Mott-insulating phase. Typical error bars for the experimental data are shown.⁴²

weight is missing; parts of the spectral weight are transferred to higher frequencies - to the Hubbard band which has more than twice the amplitude for $x = 0$ compared to $x = 0.85$ and 0.9 (see Fig. 3). However, not all the spectral weight is recovered in the Hubbard bands, but is reduced in the high- ω limit compared to the metallic compounds.

D. Electronic correlations in the vicinity of the Mott transition

In the analysis of the electrodynamics of the correlated charge carriers in κ -(BEDT-TTF) $_2$ Cu[N(CN) $_2$]Br $_x$ Cl $_{1-x}$ given above we used a multicomponent model where we separated a free-carriers zero-frequency mode and a finite-frequency mode due to transitions between Hubbard bands. However, for the low-temperature state of the metallic compounds with $x = 0.73$, 0.85 , and 0.9 , where the zero-frequency peak is strong and overlaps with the finite-frequency contributions, we may use an alternative description by a one-component model. Here, only itinerant charge carriers account for the frequency dependence of the optical conductivity shown in Fig. 3(a). The same dual approach was utilized to describe the in-plane electromagnetic response of the high- T_c cuprates.²⁴ The multicomponent model gives a reasonable description for the strongly-underdoped cuprates, while for optimally and overdoped cuprates the one-component model seems to be more appropriate.^{24,48} From the conductivity spectra we can extract the frequency dependence of scattering rate $\Gamma_1(T, \omega)$ and renormalized mass of the charge carriers which is, as well as the temperature dependence of both, governed by many-body effects.

A fingerprint of strong electron-electron interactions is the T^2 dependence of the scattering rate and consequently of the dc resistivity. For example, in the resistivity of heavy fermions a T^2 behavior was observed, however, there the experimental findings were limited

to very low temperatures and rather small temperature intervals.^{41,49} An example of a two-dimensional Fermi liquid where the in-plane and out-of-plane resistivity follows a T^2 law is Sr $_2$ RuO $_4$.⁵⁰ Transport measurements of the in-plane or out-of-plane resistivity of metallic κ -(BEDT-TTF) $_2$ Cu[N(CN) $_2$]Br or κ -(BEDT-TTF) $_2$ Cu[N(CN) $_2$]Cl with applied hydrostatic pressure also indicated $\rho \propto T^2$ in the temperature region between the superconducting transition and approximately 40 K.^{13,27,51,52,53} that was interpreted in terms of the Fermi-liquid model.¹⁸ But this conclusion was always under debate since the temperature region is very limited and other models also propose a quadratic temperature dependence of the resistivity.^{49,53,54}

Optical spectroscopy offers an alternative way to probe the electron-electron interactions. According to Fermi-liquid theory

$$\Gamma_1(T, \omega) = A [(2\pi k_B T)^2 + (\hbar\omega)^2] \quad ; \quad (3)$$

the T^2 dependence of the scattering rate $\Gamma_1 = 1/\tau$ should be accompanied by a similar parabolic frequency dependence. To extract information about the frequency-dependent scattering rate $\Gamma_1(T, \omega)$ and effective mass, we analyze the low-temperature spectra using a generalized Drude model;^{33,55} this approach is commonly applied to correlated-electron systems like heavy fermions and high-temperature superconductors.^{24,41,56,57}

$$\hat{\sigma}(\omega) = \frac{\omega_p^2}{4\pi} \frac{1}{\Gamma_1(\omega) - i\omega(m^*(\omega)/m_{b,opt})} \quad . \quad (4)$$

Here a $\Gamma_1(\omega)$ is the real part of the complex scattering rate $\hat{\Gamma}(\omega) = \Gamma_1(\omega) + i\Gamma_2(\omega)$, with the imaginary part related to the enhanced mass (renormalized due to electron-electron interactions) $m^*/m_{b,opt} = 1 - \Gamma_2(\omega)/\omega$. From the complex conductivity we obtain expressions for $\Gamma_1(\omega)$ and $m^*(\omega)$ in terms of $\sigma_1(\omega)$ and $\sigma_2(\omega)$ as follows:

$$\Gamma_1(\omega) = \frac{\omega_p^2}{4\pi} \frac{\sigma_1(\omega)}{|\hat{\sigma}(\omega)|^2} \quad ; \quad \frac{m^*(\omega)}{m_{b,opt}} = \frac{\omega_p^2}{4\pi} \frac{\sigma_2(\omega)/\omega}{|\hat{\sigma}(\omega)|^2} \quad . \quad (5)$$

Fig. 11 shows $\Gamma_1(\omega)$ and $m^*(\omega)/m_{b,opt}$ for κ -(BEDT-TTF) $_2$ Cu[N(CN) $_2$]Br $_x$ Cl $_{1-x}$ samples with Br concentrations $x \geq 0.73$. The scattering rate Γ_1 consists out of a frequency-independent part $\Gamma_1(0)$, which is derived from the limit $\omega \rightarrow 0$, and a frequency-dependent part. We obtained $\Gamma_1(0) = 315 \text{ cm}^{-1}$ ($x = 0.73$), 48 cm^{-1} ($x = 0.85$), and 280 cm^{-1} ($x = 0.9$) at $T = 5 \text{ K}$.⁵⁸ The frequency dependencies of the scattering rate and effective mass in the less correlated compounds with $x = 0.85$ and 0.9 have similar smooth characteristics as expected for a small variation in doping; $\Gamma_1(\omega)$ increases up to the maximum at a frequency ω_m and then decreases towards higher frequencies. κ -(BEDT-TTF) $_2$ Cu[N(CN) $_2$]Br $_{0.73}$ Cl $_{0.27}$, located very close to the metal-insulator transition, has a substantially enhanced scattering rate and effective mass with very strong frequency dependencies. We find the maximum in $\Gamma_1(\omega)$ that corresponds to

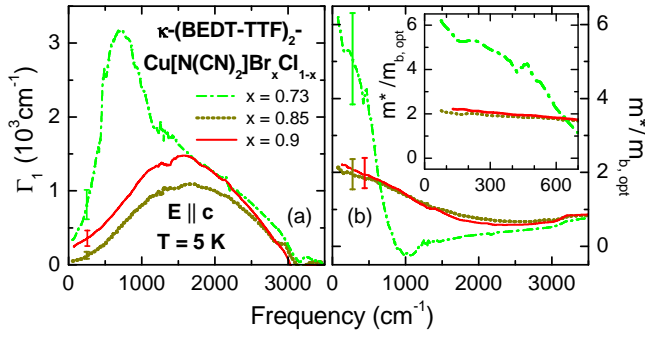


FIG. 11: (Color online) Frequency dependence of the low-temperature ($T = 5$ K) scattering rate $\Gamma_1(\omega)$ (left panel) and effective mass $m^*/m_{b,\text{opt}}$ (right panel and inset) of κ -(BEDT-TTF) $_2$ Cu[N(CN) $_2$]Br $_x$ Cl $_{1-x}$ for different x as indicated. Typical error bars for the experimental data are shown.

a drop in $m^*(\omega)/m_{b,\text{opt}}(\omega)$ at $\omega_m/(2\pi c) \approx 700$ cm^{-1} for $x = 0.73$ and $\omega_m/(2\pi c) \approx 1600$ cm^{-1} for $x = 0.85$ and 0.9 , respectively. A presence of a peak in $1/\tau(\omega)$ and a sharp drop in $m^*(\omega)$ at a certain frequency ω_m is in excellent agreement with DMFT calculations.¹⁹

The frequency-dependent part of $\Gamma_1(\omega)$ well below ω_m is analyzed in Fig. 12. All investigated metallic compositions are linear in the $[\Gamma_1 - \Gamma_1(0)]$ vs. ω^2 representation below a frequency scale ω^* , where $\omega^*/(2\pi c) \approx 500$ cm^{-1} for $x = 0.73$ and $\omega^*/(2\pi c) \approx 600$ cm^{-1} for $x = 0.85$ and 0.9 . Deviations from the ω^2 behavior of the scattering rate expected in Fermi liquids occur for $\omega > \omega^*$, with $\hbar\omega^* \ll \epsilon_F$, the Fermi energy. Thus, ω^* is a low energy scale which separates conventional metallic behavior from unconventional non-Fermi-liquid behavior at large frequencies. In agreement with our experimental values, DMFT calculations predict a red shift of ω^* and ω_m with increasing correlations U/t ; the parameters mentioned in Sec. II A 2 give a good description for $x = 0.73$ and yield $\omega^*/(2\pi c) \approx 400$ cm^{-1} .¹⁹ It should be mentioned that cluster DMFT³⁷ suggests when the phase border is approached from the metallic side an even further reduced coherence scale and a coexistence region of the metallic and insulating phases due to short-range correlations in the anomalous metallic state with a non-quadratic scattering rate. Since there are no indications of such a behavior in the data presented in this work, we conclude that the U/t and T/t range of our experiments does not cover the coexistence region.

Generally, it is predicted by Brinkman-Rice theory^{4,59} and DMFT calculations¹⁵ that the electronic correlations become stronger on approaching the Mott transition from the metallic side. Accordingly, the effective mass gets enhanced. Resonating-valence-bond theory of the Hubbard-Heisenberg model predicts a gradual increase of m^* for values of effective repulsion U/t not too close to the first-order Mott transition and a strong increase very close to the transition.⁴⁴ We find a mass enhancement (inset of Fig. 11, $\omega^*/(2\pi c) < 300$ cm^{-1}) of about a factor 2 in the less correlated compounds and of about 5-6

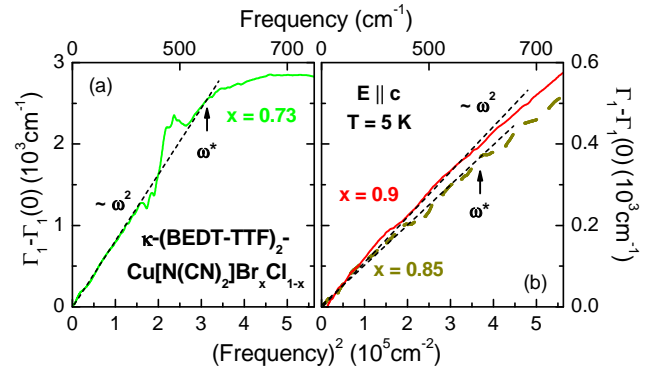


FIG. 12: (Color online) Frequency-dependent part of the scattering rate $\Gamma_1(\omega) - \Gamma_1(0)$ at $T = 5$ K of κ -(BEDT-TTF) $_2$ Cu[N(CN) $_2$]Br $_x$ Cl $_{1-x}$ as function of the squared frequency. We determined for the frequency-independent dc limit of the scattering rate $\Gamma_1(0)$ the following values : 315 cm^{-1} ($x = 0.73$), 48 cm^{-1} ($x = 0.85$), and 280 cm^{-1} ($x = 0.9$). Note the different vertical scales for both frames.

in the material located very close to the Mott transition, which is in accord with the theoretical prediction.

The slope a in the linear regions of $[\Gamma_1 - \Gamma_1(0)]$ plotted vs. ω^2 in Fig. 12 is proportional to the prefactor A in Eq. (3). In Fermi liquids, A is related to the mass enhancement by $A \propto (m^*)^2$, which leads to the well-known Kadowaki-Woods ratio $A/\gamma^2 = \text{const.}$ via $\gamma \propto m^*$, where γ is the Sommerfeld coefficient.⁶⁰ The comparative mass enhancement in the low-frequency limit $m^*(x = 0.73)/m^*(x = 0.85) \approx 2.75$ and the enhancement of the prefactor obtained from the scattering rate $A(x = 0.73)/A(x = 0.85) \approx 8$ evidences the excellent fulfilment of this relation. It should be noted, however, that pressure-dependent dc measurements of the in-plane resistivity in κ -(BEDT-TTF) $_2$ Cu[N(CN) $_2$]Cl yield a prefactor of T^2 at low temperatures that changes by a factor of three when pressure is increased from 300 bar to 1 kbar.¹³ If we compare the data of the samples with $x = 0.85$ and $x = 0.9$ in Figs. 11 and 12, it is obvious that A and m^* are about the same in both as expected for a small variation in doping.⁵⁸ According to the relations $A \propto (m^*)^2 \propto (T_F^*)^{-2}$, the prefactor A and m^* are also expected to scale with the effective Fermi temperature T_F^* .⁵³ If we associate T_F^* with the energy scale below which we observe the ω^2 dependence, i.e. ω^* , we cannot identify such a scaling. Interestingly, the energy scale ω_m , which marks the maximum in $\Gamma_1(\omega)$, seems to fulfil this relation much better.

The strong mass renormalization which we note in the bandwidth-controlled Mott transition in κ -(BEDT-TTF) $_2$ Cu[N(CN) $_2$]Br $_x$ Cl $_{1-x}$ is in contrast to observations in two-dimensional doped Mott insulators like the cuprates where the Mott transition is obtained by band-filling control.⁴⁷ There, the transition into the Mott-insulating state is of the vanishing-carriers type and the effective mass stays constant. An investigation of the evolution of the effective mass close to the Mott transition

in $V_{2-y}O_3$ confirmed that the effective mass diverged as function of hydrostatic pressure while it slightly decreased as function of hole doping y if the metal-insulator transition was approached.⁶¹

III. CONCLUSION

The polarized reflection spectra of κ -(BEDT-TTF)₂-Cu[N(CN)₂]Br_xCl_{1-x} have been systematically investigated in a frequency range from the very far-infrared to the near-infrared. This series of alloys is a benchmark system for the bandwidth-controlled Mott transition, with U/t decreasing as function of Br content x . In the present study we follow the correlation and temperature dependence of the correlated-carriers dynamical response on both sides of the Mott transition. We compare the findings with predictions of the single-site and cluster DMFT calculations for a half-filled Hubbard model.

At elevated temperatures $T \gg 50$ K, all compounds are narrow-gap semiconductors and show no substantial differences in the optical spectra. The Mott-Hubbard physics is confined to low temperatures $T < 50$ K: in the Br-rich samples, the zero-frequency quasiparticle peak accounts for the metallic conductivity. With increasing U/t , the Drude spectral weight is suppressed and totally vanishes beyond the first-order phase transition

at $x_c \approx 0.7$ in accord with theoretical predictions. In the Cl-rich Mott-insulating samples, an energy gap opens and increases as the electronic correlations get stronger and reaches almost 1000 cm^{-1} for $T \rightarrow 0$ in the pristine Cl compound. The enhanced U/t thus results in a redistribution and suppression of the spectral weight of the correlated charge carriers, including the transitions between the Hubbard bands and, if present, the Drude weight. Below a characteristic frequency $\omega^*/(2\pi c) \approx 500 - 600 \text{ cm}^{-1}$, the quasiparticles in the metallic phase show typical signatures of a Fermi liquid: a $A\omega^2$ dependence of the scattering rate $\Gamma_1(\omega)$ and a substantial enhancement of the effective mass $m^*(\omega)$, where the prefactor A and $m^*(\omega \rightarrow 0)$ follow the $A \propto (m^*)^2$ scaling. Both parameters diverge as x_c is approached. Above ω^* , a transition to an unconventional non-Fermi liquid regime is observed.

Acknowledgments

We thank J. Merino and R. McKenzie for helpful discussions of theoretical aspects. The project was supported by the Deutsche Forschungsgemeinschaft. ND is grateful for the support by the Alexander von Humboldt-Foundation and by the Magarete-von-Wrangell-Programm of Baden-Württemberg.

-
- ¹ N.F. Mott, *Metal-Insulator Transitions* (Taylor & Francis, London, 1974); F. Gebhard, *The Mott Metal-Insulator Transition* (Springer, Berlin, 1997).
- ² P. Fulde, *Electron Correlations in Molecules and Solids*, 3rd edition (Springer-Verlag, Berlin, 2002).
- ³ N. Grewe and F. Steglich, in: *Handbook on the Physics and Chemistry of Rare Earths*, V. **14**, ed.: K.A. Gscheidner Jr. and L. Eyring (Elsevier, Amsterdam - New York, 1991), p. 343.
- ⁴ M. Imada, A. Fujimori, and Y. Takura, *Rev. Mod. Phys.* **63**, 1 (1998).
- ⁵ D. Jérôme, in *Organic Conductors*, edited by J.-P. Farges (Marcel Dekker, New York, 1994), p. 405.
- ⁶ T. Ishiguro, K. Yamaji, and G. Saito, *Organic Superconductors*, 2nd edition (Springer-Verlag, Berlin, 1998).
- ⁷ R.H. McKenzie, *Comments Cond. Mat.* **18**, 309 (1998).
- ⁸ H. Seo, C. Hotta, and H. Fukuyama, *Chem. Rev.* **104**, 5005 (2004).
- ⁹ M. Dressel and N. Drichko, *Chem. Rev.* **104**, 5689 (2004).
- ¹⁰ H. Fukuyama, *J. Phys. Soc. Jpn.* **75**, 051001 (2006).
- ¹¹ BEDT-TTF stands for bis-(ethylenedithio)tetrathiafulvalene.
- ¹² S. Lefebvre, P. Wzietek, S. Brown, C. Bourbonnais, D. Jérôme, C. Mézière, M. Fourmigué, and P. Batail, *Phys. Rev. Lett.* **85**, 5420 (2000).
- ¹³ P. Limelette, P. Wzietek, S. Florens, A. Georges, T.A. Costi, C. Pasquier, D. Jerome, C. Mézière, and P. Batail, *Phys. Rev. Lett.* **91**, 016401 (2003).
- ¹⁴ F. Kagawa, T. Itou, K. Miyagawa, and K. Kanoda, *Phys. Rev. B* **69**, 064511 (2004); F. Kagawa, T. Itou, K. Miyagawa, and K. Kanoda, *Phys. Rev. Lett.* **93**, 127001 (2004); F. Kagawa, K. Miyagawa, and K. Kanoda, *Nature* **436**, 534 (2005).
- ¹⁵ A. Georges, G. Kotliar, W. Krauth, and M.J. Rozenberg, *Rev. Mod. Phys.* **68**, 13 (1996).
- ¹⁶ G. Kotliar and D. Vollhardt, *Physics Today*, March 2004, p. 53.
- ¹⁷ H. Kino and H. Fukuyama, *J. Phys. Soc. Jpn.* **64**, 2726 (1995); *ibid.* **64**, 4523 (1995); *ibid.* **65**, 2158 (1996).
- ¹⁸ J. Merino and R. H. McKenzie, *Phys. Rev. B* **61**, 7996 (2000); *ibid.* **62**, 16442 (2000).
- ¹⁹ J. Merino, M. Dumm, N. Drichko, M. Dressel, and R.H. McKenzie, *Phys. Rev. Lett.* **100**, 086404 (2008).
- ²⁰ J. E. Eldridge, K. Kornelsen, H. H. Wang, J. M. Williams, A. V. D. Crouch, and D. M. Watkins, *Solid State Commun.* **79**, 583 (1991).
- ²¹ K. Kornelsen, J. E. Eldridge, H. H. Wang, H. A. Charlier, and J. M. Williams, *Solid State Commun.* **81**, 343 (1992).
- ²² P. Haas, E. Griesshaber, B. Gorshunov, D. Schweitzer, M. Dressel, T. Klaus, W. Strunz, and F. F. Assaad, *Phys. Rev. B* **62**, R14673 (2000).
- ²³ M. Dressel, N. Drichko, J. Schlueter, and J. Merino, *Phys. Rev. Lett.* **90**, 167002 (2003).
- ²⁴ D.N. Basov and T. Timusk, *Rev. Mod. Phys.* **77**, 721 (2005).
- ²⁵ N. Drichko, M. Dressel, C. A. Kuntscher, A. Pashkin, A. Greco, J. Merino, and J. Schlueter *Phys. Rev. B* **74**, 235121 (2006).
- ²⁶ T. Sasaki, N. Yoneyama, Y. Nakamura, N. Kobayashi, Y. Ikemoto, T. Moriwaki, and H. Kimura, *Phys. Rev. Lett.*

- 101**, 206403 (2008).
- ²⁷ D. Faltermeier, J. Barz, M. Dumm, M. Dressel, N. Drichko, B. Petrov, V. Semkin, R. Vlasova, C. Méziere, and P. Batail, *Phys. Rev. B* **76**, 165113 (2007).
- ²⁸ M.J. Rice, *Phys. Rev. Lett.* **37**, 36 (1976).
- ²⁹ Delhaes P., Yartsev V.M., *Advances in Spectroscopy*, **22**, R.J.H. Clark, R.E. Hester Eds. *John Wiley and Sons*, 1993, p. 199; V. M. Yartsev, O. Fichet, J.-P. Borgion and P. Delhaes. *J. Phys. II France* **3**, 647 (1993)
- ³⁰ V.M Yartsev , O.O. Drozdova, V.N. Semkin and R.M. Vlasova, *J. Phys. I (France)* **6**, 1673 (1996); V.M. Yartsev, in: *Materials and Measurements in Molecular Electronics*, ed. by K. Kajimura and S. Kanoda (Springer-Verlag, Berlin 1996), p. 189; V. M. Yartsev and A. Graja, *Int. Journ. of Mod. Phys. B* **12**, 1643 (1998).
- ³¹ M. Dressel D. Faltermeier, M. Dumm, N. Drichko, B. Petrov, V. Semkin, R. Vlasova, C. Méziere, and P. Batail, *Physica B* **404**, 541 (2009).
- ³² Here we should note that the substitution of Cl by Br in the anion layers does not simply and homogeneously reduce the lattice parameters. In the table below the unit cell parameters and volume of κ -(BEDT-TTF)₂Cu[N(CN)₂]Cl and κ -(BEDT-TTF)₂Cu[N(CN)₂]Br are determined at room temperature. The overlap integrals t are given at $T = 127$ K.^{8,62}
- | X | κ -(BEDT-TTF) ₂ Cu[N(CN) ₂]X | |
|-----------------------|--|--------|
| | Cl | Br |
| a (Å) | 12.977 | 12.942 |
| b (Å) | 29.979 | 30.016 |
| c (Å) | 8.480 | 8.539 |
| V (Å ³) | 3299 | 3317 |
| t_1 (meV) | 26 | 25 |
| t_2 (meV) | 36 | 38 |
- In fact while a decreases when going from κ -(BEDT-TTF)₂Cu[N(CN)₂]Cl to κ -(BEDT-TTF)₂Cu[N(CN)₂]Br, the c axis increases, leading to stronger frustration for κ -(BEDT-TTF)₂Cu[N(CN)₂]Br. This effect might be of superior importance for formation of the coherent particles.
- ³³ M. Dressel and G. Grüner, *Electrodynamics of Solids* (Cambridge University Press, Cambridge, 2002).
- ³⁴ At $T = 300$ K, the spectral weight is not completely recovered in most of the compositions. At least parts of the missing weight can be attributed to the substantial thermal expansion of the crystals. When heated up from 20 K to 295 K, the volume of κ -(BEDT-TTF)₂Cu[N(CN)₂]Br increases by about 3%.⁶³
- ³⁵ M.J. Rozenberg, G. Kotliar, H. Kajueter, G.A. Thomas, D.H. Rapkine, J.M. Honig, and P. Metcalf, *Phys. Rev. Lett.* **75**, 105 (1995).
- ³⁶ B. Kyung, S.S. Kancharla, D. Sénéchal, A.-M. S. Tremblay, M. Civelli, and G. Kotliar, *Phys. Rev. B* **73**, 165114 (2006); B. Kyung and A.-M. S. Tremblay, *Phys. Rev. Lett.* **97**, 046402 (2006).
- ³⁷ H. Park, K. Haule, and G. Kotliar, *Phys. Rev. Lett.* **101**, 186403 (2008).
- ³⁸ T. Ohashi, T. Momoi, H. Tsunetsugu, and N. Kawakami, *Phys. Rev. Lett.* **100**, 076402 (2008).
- ³⁹ Park *et al.* call it a “bad insulator”.³⁷
- ⁴⁰ R. Bulla, T.A. Costi, and D. Vollhardt, *Phys. Rev. B* **64**, 045103 (2001).
- ⁴¹ L. Degiorgi, *Rev. Mod. Phys.* **71**, 687 (1999).
- ⁴² In the analysis given in Section IID we will attribute the discrepancy between the $x = 0.85$ and 0.9 data to the different frequency-independent parts of the scattering rate $\Gamma_1(0)$ in both compounds (see also Ref. 58).
- ⁴³ M. Capone, L. Capriotti, F. Becca, S. Caprara, *Phys. Rev. B* **63**, 085104 (2001).
- ⁴⁴ B.J. Powell and R.H. McKenzie, *Phys. Rev. Lett.* **94**, 047004 (2005).
- ⁴⁵ P.F. Maldague, *Phys. Rev. B* **16**, 2437 (1977).
- ⁴⁶ S. Uchida, T. Ido, H. Takagi, T. Arima, Y. Tokura and S. Tajima, *Phys. Rev. B* **43**, 7942 (1991).
- ⁴⁷ W.J. Padilla, Y.S. Lee, M. Dumm, G. Blumberg, S. Ono, Kouji Segawa, Seiki Komiya, Yoichi Ando, D.N. Basov, *Phys. Rev. B* **72**, 060511(R) (2005).
- ⁴⁸ Y.S. Lee *et al.*, *Phys. Rev. B* **72**, 054529 (2005).
- ⁴⁹ G.R. Stewart, *Rev. Mod. Phys.* **56**, 755 (1984).
- ⁵⁰ Y. Maeno *et al.*, *J. Phys. Soc. Jpn.* **66**, 1405 (1997).
- ⁵¹ M. Dressel, S. Bruder, G. Grüner, K.D. Carlson, H.H. Wang, and J.M. Williams, *Phys. Rev. B* **48**, 9906 (1993); M. Dressel, O. Klein, G. Grüner, K.D. Carlson, H.H. Wang, and J.M. Williams, *Phys. Rev. B* **50**, 13603 (1994).
- ⁵² M. Dressel and G. Grüner, *Mol. Cryst. Liq. Cryst.* **248**, 107 (1996).
- ⁵³ Ch. Strack, C. Akinci, V. Paschenko, B. Wolf, E. Uhrig, W. Assmus, M. Lang, J. Schreuer, L. Wiehl, J.A. Schlueter, J. Wosnitza, D. Schweitzer, J. Müller, and J. Wykoff, *Phys. Rev. B* **72**, 054511 (2005).
- ⁵⁴ M. Weger and D. Schweitzer, *Synth. Met.* **70**, 889 (1995); J. Hagel, J. Wosnitza, C. Pfeleiderer, J. A. Schlueter, J. Mohtasham, and G. L. Gard, *Phys. Rev. B* **68**, 104504 (2003).
- ⁵⁵ J.W. Allen and J.C. Mikkelsen, *Phys. Rev. B* **15**, 2952 (1977).
- ⁵⁶ M. Dressel, N.V. Kasper, K. Petukhov, B. Gorshunov, G. Grüner, M. Huth, and H. Adrian, *Phys. Rev. Lett.* **88**, 186404 (2002); M. Dressel, N.V. Kasper, K. Petukhov, D.N. Peligrad, B. Gorshunov, M. Jourdan, M. Huth, and H. Adrian, *Phys. Rev. B* **66**, 035110 (2002).
- ⁵⁷ S.V. Dordevic and D.N. Basov, *Ann. Physik* **15**, 545 (2006).
- ⁵⁸ The enhancement of $\Gamma_1(0)$ by a factor of about 6 observed in the $x = 0.9$ sample (compared to $x = 0.85$) might originate from the presence of more crystal imperfections. Indeed, the surface of the $x = 0.9$ crystals was not as shiny as e.g. that of the $x = 0.85$ crystals. The higher $\Gamma_1(0)$ also results in the lower amplitude and larger width of the Drude peak observed in σ_1 of $x = 0.9$ if compared to $x = 0.85$ (inset of Fig. 8) which also results in a considerable reduction of J_c of the correlated carriers seen in Figs. 8 and 10 in the limit of low T . Since the dynamical properties of the correlated carriers are not influenced, the $x = 0.9$ sample still gives very valuable information for our analysis.
- ⁵⁹ W.F. Brinkman and T.M. Rice, *Phys. Rev. B* **2**, 4302 (1970).
- ⁶⁰ K. Kadowaki and S.B. Woods, *Solid State Commun.* **58**, 507 (1986).
- ⁶¹ S.A. Carter, T.F. Rosenbaum, P. Metcalf, J.M. Honig, and J. Spalek, *Phys. Rev. B* **48**, 16841 (1993).
- ⁶² T. Mori, H. Mori, and S. Tanaka, *Bull. Chem. Soc. Jpn.* **72**, 179 (1999).
- ⁶³ Y. Watanabe, H. Seo, T. Sasaki, and N. Toyota, *J. Phys. Soc. Jpn.* **60**, 3608 (1991).